ACS chemical biology

Articles

Cite This: ACS Chem. Biol. 2019, 14, 266−275

pubs.acs.org/acschemicalbiology

Crystal Structures of Fumarate Hydratases from *Leishmania major* in a Complex with Inhibitor 2-Thiomalate

Patricia R. Feliciano,[†,‡,§,∥] Catherine L. Drennan,*[,†,‡,§] and Maria Cristina Nonato*[,∥]

[†]Howard Hughes Medical Institute, Massachusetts Institute of Technology, Cambridge, Massachusetts 02139, United States

[‡]Department of Biology, Massachusetts Institute of Technology, Cambridge, Massachusetts 02139, United States

[§]Department of Chemistry, Massachusetts Institute of Technology, Cambridge, Massachusetts 02139, United States

[∥]Laboratório de Cristalografia de Proteínas, Faculdade de Ciências Farmacêuticas de Ribeirão Preto, Universidade de São Paulo, São Paulo 14040-903, Brazil

Supporting Information

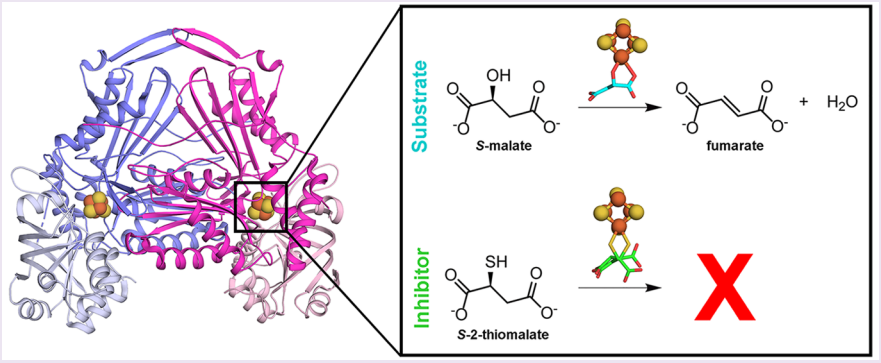

ABSTRACT: Leishmaniases affect the poorest people on earth and have no effective drug therapy. Here, we present the crystal structure of the mitochondrial isoform of class I fumarate hydratase (FH) from *Leishmania major* and compare it to the previously determined cytosolic *Leishmania major* isoform. We further describe the mechanism of action of the first class-specific FH inhibitor, 2-thiomalate, through X-ray crystallography and inhibition assays. Our crystal structures of both FH isoforms with inhibitor bound at 2.05 Å resolution and 1.60 Å resolution show high structural similarity. These structures further reveal that the selectivity of 2-thiomalate for class I FHs is due to direct coordination of the inhibitor to the unique Fe of the catalytic [4Fe-4S] cluster that is found in class I parasitic FHs but is absent from class II human FH. These studies provide the structural scaffold in order to exploit class I FHs as potential drug targets against leishmaniases as well as Chagas diseases, sleeping sickness, and malaria.

Leishmaniases are neglected tropical diseases (NTDs) caused by the parasite *Leishmania* spp. There are three clinical forms of leishmaniases: cutaneous, muco-cutaneous, and visceral. Cutaneous, the most common form of the disease, and muco-cutaneous leishmaniases can be caused by *L. major*, *L. panamensis*, *L. mexicana*, *L. braziliensis*, *L. infantum*, and *L. guyanensis*, among other species. The visceral leishmaniasis, the most severe form of the disease, is caused by *L. donovani*, *L. tropica*, or *L. infantum*. Leishmaniases are a major public health problem in low-income countries with approximately 1.3 million new cases and over 20 000 deaths annually, according to the World Health Organization. The control of this disease is challenging due to the growing number of cases in the past 2 decades as a consequence of poverty, climatic and environmental changes, coinfection with HIV, conflict areas, migratory flow, and rapid urbanization.[1,2] A vaccine is not yet available to prevent leishmaniases, and the current treatment is limited to drugs with poor efficacy, high toxicity, high cost, long duration, and/or the requirement of daily injections.[3] Development of resistance to the available drugs is also becoming an issue.[3] Consequently, more effective therapies are needed to fight leishmaniases.

Fumarate hydratase (FH; fumarase; EC 4.2.1.2) catalyzes the stereospecific reversible conversion of fumarate to *S*-malate. This reaction is part of the tricarboxylic acid (TCA) cycle, participates in the succinic fermentation pathway[4] and DNA repair,[5] and is proposed to provide fumarate for the *de novo* pyrimidine biosynthetic pathway.[6] FHs are grouped in two classes with low amino acid sequence identity (~20%) and distinct protein structures.[7,8] Class I FHs are [4Fe-4S] cluster-containing dimeric enzymes found in archaea, prokaryotes, and unicellular eukaryotes, including protozoan parasites.[9−11] Class II FHs are iron-independent tetrameric enzymes found in prokaryotes and eukaryotes, including humans.[12] Thus, class I

Received: October 31, 2018
Accepted: January 15, 2019
Published: January 15, 2019

DOI: 10.1021/acschembio.8b00972
ACS Chem. Biol. 2019, 14, 266−275

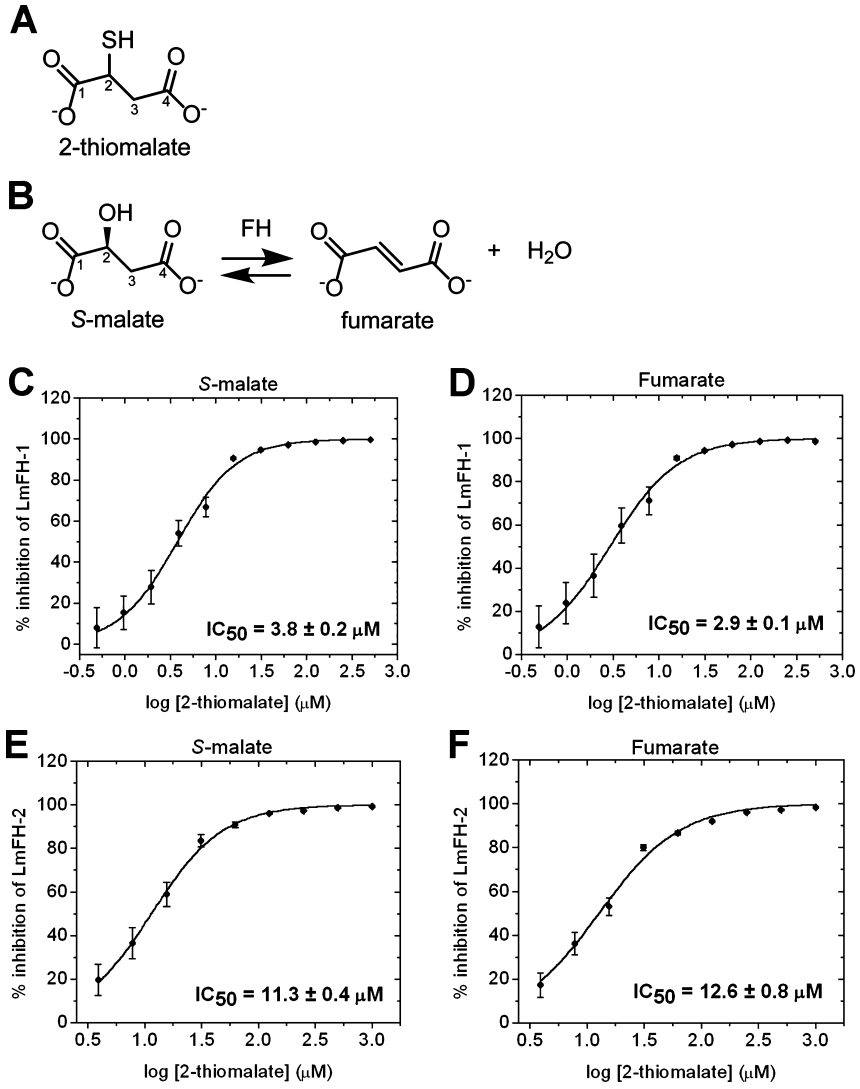

Figure 1. Inhibition of LmFH isoforms by 2-thiomalate. (A) Structure of 2-thiomalate molecule. (B) FH catalytic reversible reaction of *S*-malate to fumarate. (C) Dose−response curve of the inhibition of mitochondrial LmFH-1 by *RS*-2-thiomalate against *S*-malate (3 mM). (D) Dose−response curve of the inhibition of mitochondrial LmFH-1 by *RS*-2-thiomalate against fumarate (3 mM). (E) Dose−response curve of the inhibition of cytosolic LmFH-2 by *RS*-2-thiomalate against *S*-malate (3 mM). (F) Dose−response curve of the inhibition of cytosolic LmFH-2 by *RS*-2-thiomalate against fumarate (6 mM). Error bars represent three independent measurements.

FHs are considered attractive drug targets because they are structurally distinct from class II human FH and play vital roles in multiple metabolic pathways.

Leishmania major expresses two isoforms of class I FHs: mitochondrial LmFH-1 (60.8 kDa) and cytosolic LmFH-2 (62.6 kDa),[9] which share 59% of sequence identity. The crystal structure of LmFH-2 was previously determined in a complex with substrate *S*-malate, revealing bidentate coordination of substrate to the unique Fe of the catalytic [4Fe-4S] cluster.[7] Here, we report the crystal structures of LmFH-1 and LmFH-2 in a complex with an inhibitor, 2-thiomalate, an analogue of the substrate *S*-malate. We further report that 2-thiomalate is a micromolar inhibitor of both LmFH isoforms. Recently it was shown that 2-thiomalate is also a micromolar inhibitor of class I FHs from parasites *Trypanosoma cruzi* and *Plasmodium falciparum* but does not inhibit human FH.[10,11] To our knowledge, 2-thiomalate is the first selective small molecule inhibitor of class I FHs, and here we show that this selectivity arises from the binding of the inhibitor to the class I FH catalytic [4Fe-4S] cluster; the human class II FH does not utilize a [4Fe-4S] cluster. In addition, LmFH-1 and LmFH-2 structures show high structural similarity, indicating that inhibitors of one isoform are likely to inhibit the other isoform. Our data reveal the mechanism of action of 2-thiomalate as well as implicate class I FHs as valuable therapeutic targets for the development of new drugs against leishmaniases and possibly Chagas diseases, sleeping sickness, and malaria.

RESULTS

Inhibition of LmFH Isoforms by 2-Thiomalate. The small molecule 2-thiomalate (Figure 1A) is an analogue of the substrate *S*-malate (Figure 1B) and has been identified as a micromolar competitive inhibitor of class I parasitic FHs but does not affect the activity of class II human FH.[10,11] Here, we examine the ability of *RS*-2-thiomalate to inhibit LmFH activity in both directions of this reversible reaction (Figure 1B) and for both the mitochondrial and cytosolic LmFH isoforms. Although the ability of *RS*-2-thiomalate to cross the

DOI: 10.1021/acschembio.8b00972
ACS Chem. Biol. 2019, 14, 266−275

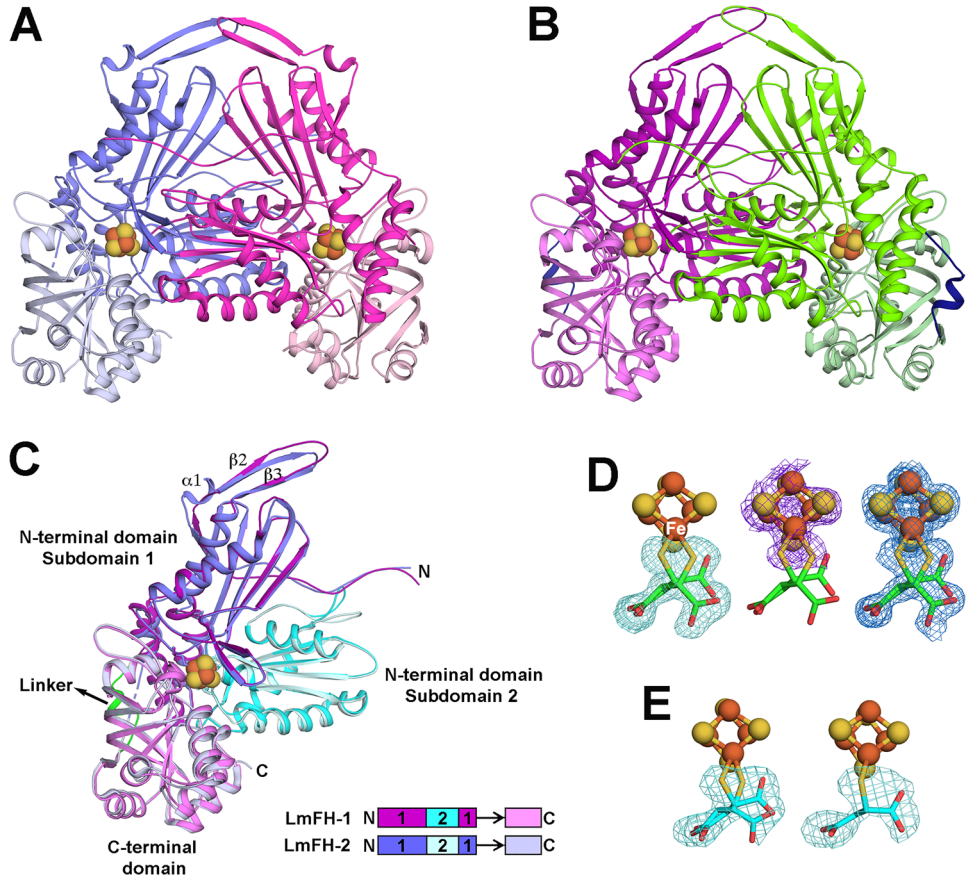

Figure 2. Crystal structures of LmFH isoforms in a complex with 2-thiomalate. (A) Overall structure of cytosolic LmFH-2 functional dimer. Monomers are shown in blue (chain A) and pink (chain B) and are comprised of two domains: N-terminal domain (darker blue and pink) and C-terminal domain (lighter blue and pink) connected by a flexible linker. (B) Overall structure of mitochondrial LmFH-1 functional dimer. Monomers are shown in purple (chain A) and green (chain B). N-terminal domain is shown in darker purple and green, and C-terminal domain is shown in lighter purple and green. The domain linker is shown in dark blue. (C) Ribbon diagram of the superposition of LmFHs monomers (chain A). The N-terminal domain is divided into two nonsequential subdomains 1 (purple in LmFH-1 and blue in LmFH-2) and 2 (cyan in LmFH-1 and light cyan in LmFH-2), connected to C-terminal domain (light purple in LmFH-1 and light blue in LmFH-2) by a linker (green in LmFH-1 and black arrow in LmFH-2 to where linker would be if it was ordered). Linear schematic indicates subdomain order. (D) LmFH-2 in a complex with *S*-2-thiomalate. The left panel shows the $F_o - F_c$ difference electron density map contoured at 3.0 rmsd (green mesh) for *S*-2-thiomalate (green) suggesting its double conformation. The center panel shows the sulfur anomalous difference electron density map contoured at 3.0 rmsd (purple mesh) supporting the assignment of *S*-2-thiomalate (green) double conformation. The C2-thiol groups (yellow) are coordinated to the unique Fe (labeled in white) of the [4Fe-4S] cluster. The right panel shows the final $2F_o - F_c$ electron density map contoured at 1.5 rmsd (blue mesh) for *S*-2-thiomalate (green) and [4Fe-4S] cluster. (E) LmFH-1 in a complex with *S*-2-thiomalate. The left panel shows the $F_o - F_c$ difference electron density map contoured at 3.0 rmsd (green mesh) for *S*-2-thiomalate (cyan) in chains A and B, consistent with a double conformation. The right panel shows the $F_o - F_c$ difference electron density map contoured at 3.0 rmsd (green mesh) for *S*-2-thiomalate (cyan) in chains C and D, consistent with a single conformation. The catalytic [4Fe-4S] clusters are shown in orange (Fe) and yellow (S) spheres.

mitochondrial membrane has not been directly demonstrated, malate is known to cross the mitochondrial membrane,[13] encouraging our study of the mitochondrial system. The half maximal inhibitory concentration (IC_{50}) for *RS*-2-thiomalate against substrates *S*-malate and fumarate was calculated by a dose−response curve for mitochondrial isoform LmFH-1 (Figure 1C,D) and cytosolic isoform LmFH-2 (Figure 1E,F). The IC_{50} values for *RS*-2-thiomalate for LmFH-1 and LmFH-2 against *S*-malate are 3.8 ± 0.2 μM and 11.3 ± 0.4 μM and against fumarate are 2.9 ± 0.1 μM and 12.6 ± 0.8 μM, respectively. These results show that the IC_{50} values of LmFH-2 are approximately 3- and 4-fold higher than for LmFH-1 for *S*-malate and fumarate, respectively. The Web server IC_{50}-to-K_i[14] was used to estimate the apparent inhibitory constant ($K_{i,app}$) for *RS*-2-thiomalate against both substrates. The $K_{i,app}$ values for *RS*-2-thiomalate for LmFH-1 and LmFH-2 against *S*-malate are approximately 3.0 μM and 8.9 μM and against fumarate are approximately 2.5 μM and 8.2 μM, respectively. For this study, we used an apparent 50:50 racemic mixture of *RS*-2-thiomalate (Figure S1A), but the crystallographic analyses described below is consistent with the binding of only the *S*-enantiomer. Thus, the "true" IC_{50} values could be half of those determined in this study. As a control, we investigated if *RS*-2-thiomalate could be a substrate for LmFH isoforms by spectrophotometrically measuring the production of fumarate at 250 nm. As expected, no fumarate was detected, indicating that 2-thiomalate is not a substrate for LmFHs (Figure S1B).

Crystal Structure of LmFH-2 with 2-Thiomalate. The enzyme LmFH-2 has been previously crystallized in anaerobic conditions.[7] To obtain atomic information about the enzyme−inhibitor complex, we cocrystallized LmFH-2 in the presence of the inhibitor *RS*-2-thiomalate. The crystal structure of LmFH-2 in a complex with 2-thiomalate (LmFH-2-thio) was

DOI: 10.1021/acschembio.8b00972
ACS Chem. Biol. 2019, 14, 266−275

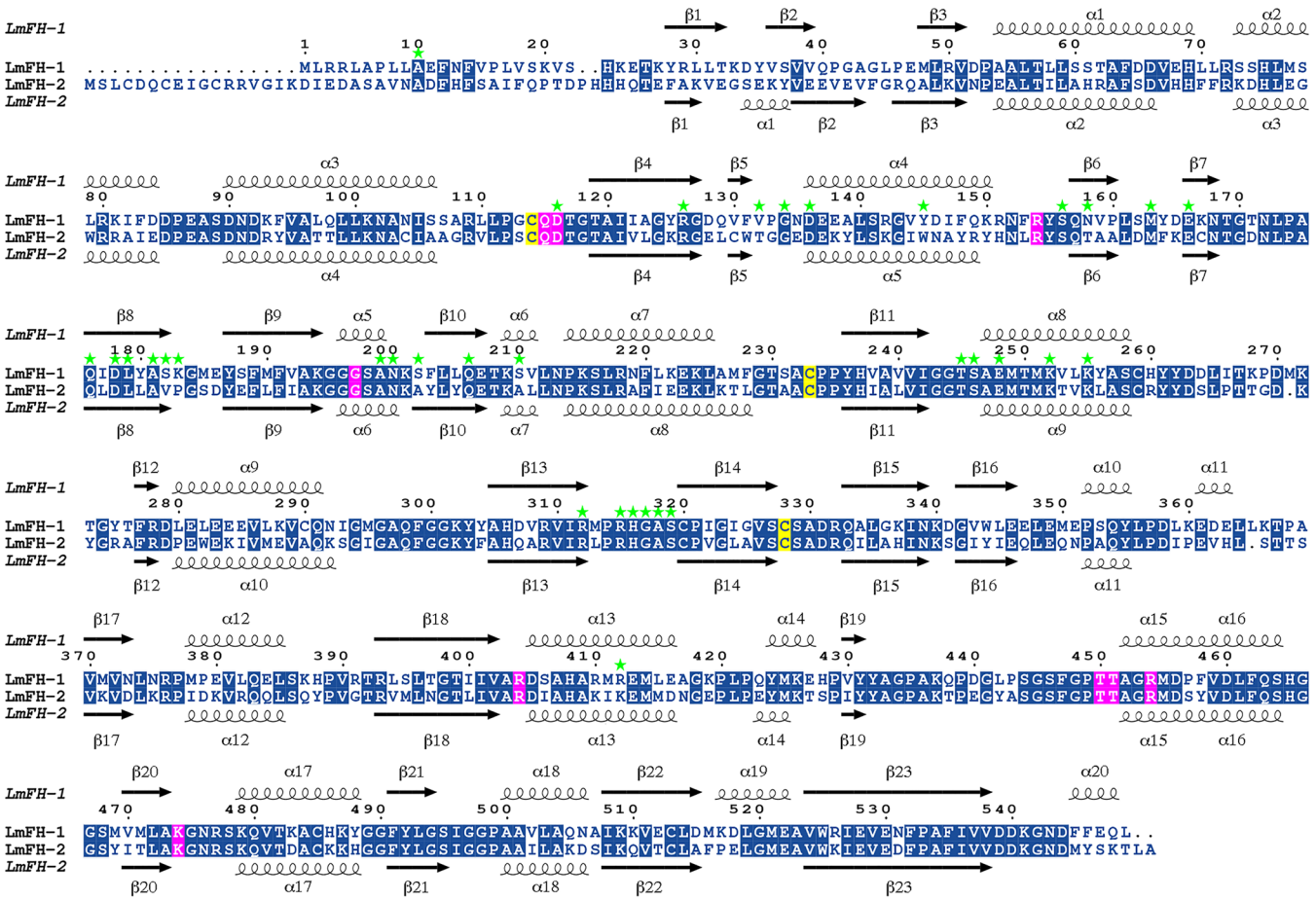

Figure 3. Sequence alignment of LmFH isoforms. LmFH-1 and LmFH-2 are the mitochondrial and cytosolic isoforms of *Leishmania major*, respectively. The conserved residues are indicated in the blue boxes. The conserved active site residues among class I FHs that coordinate to inhibitor *S*-2-thiomalate are indicated in the pink boxes. The three conserved cysteine residues, which are shown to bind a [4Fe-4S] cluster, are indicated in the yellow boxes. Secondary structures of LmFH-1 and LmFH-2 are shown on top and at the bottom of sequence alignment, respectively. The dimer interface residues of LmFH-1 are indicated in green stars. The alignment was performed using MULTALIN[15] and graphically displayed using ESPript.[16]

solved by molecular replacement using LmFH-2 structure (PDB ID code 5L2R[7]) as the search model and refined to 1.60 Å resolution (Table S1). The asymmetric unit contains one copy of the functional homodimeric enzyme, and the monomers are related by a noncrystallographic 2-fold axis (Figure 2A). The two chains are highly similar to each other and also to the two chains of the previously solved LmFH-2 structure, with rmsds for the Cα atoms of 0.2 Å. As previously described,[7] LmFH-2 is a homodimeric enzyme with each monomer comprised of two domains (N- and C-terminal domains) that are arranged around the catalytic [4Fe-4S] cluster. The N-terminal domain is divided into two non-sequential subdomains 1 and 2 and is connected to the C-terminal domain by a flexible linker (Figure 2C). The first 27 residues (Met1 to Ala27) and linker residues from Asp376 to Thr384 (chain A)/Thr385 (chain B) were excluded from the structure due to the lack of interpretable electron density.

A $F_o - F_c$ difference electron density map indicates that the 2-thiomalate is coordinated to the [4Fe-4S] cluster (Figure 2D), revealing the molecular basis for enzyme inhibition. To pinpoint the position of the C2-thiol group of 2-thiomalate (Figure 1A), sulfur anomalous data were collected at a wavelength of 1.7969 Å (LmFH-2-thio-S-peak; Table S1). If we model the *R*-enantiomer of 2-thiomalate such that the thiol group is in the sulfur anomalous density peak, the remainder of the molecule is not a good fit to the electron density map (Figure S2A). If we instead attempt to maximize the fit of the *R*-enantiomer to the observed electron density, then we find the sulfur atom of the thiol group is far from the sulfur anomalous density (Figure S2B). In contrast, there are two orientations of the *S*-enantiomer that position the thiol group in the anomalous density and show reasonable fits for the remaining atoms of 2-thiomalate (Figure 2D). Difference density, $2F_o - F_c$ electron density, and anomalous density are all best explained by a combination of both orientations of the *S*-2-thiomalate with thiol ligation of the [4Fe-4S] (Figure 2D).

Crystal Structure of LmFH-1 with 2-Thiomalate. To validate the binding mode of 2-thiomalate to both LmFH isoforms, the mitochondrial isoform LmFH-1 was also cocrystallized with *RS*-2-thiomalate. The crystal structure of LmFH-1 in a complex with 2-thiomalate (LmFH-1-thio) was solved by molecular replacement using the cytosolic isoform LmFH-2 structure (PDB code 5L2R[7]) as the search model and refined to 2.05 Å resolution (Table S1). The asymmetric unit contains two copies of the functional homodimeric enzyme (chains A and B, C and D), with monomers related by a noncrystallographic 2-fold axis (Figure 2B). The superposition of Cα atoms between monomers shows high level of structural

DOI: 10.1021/acschembio.8b00972
ACS Chem. Biol. 2019, 14, 266−275

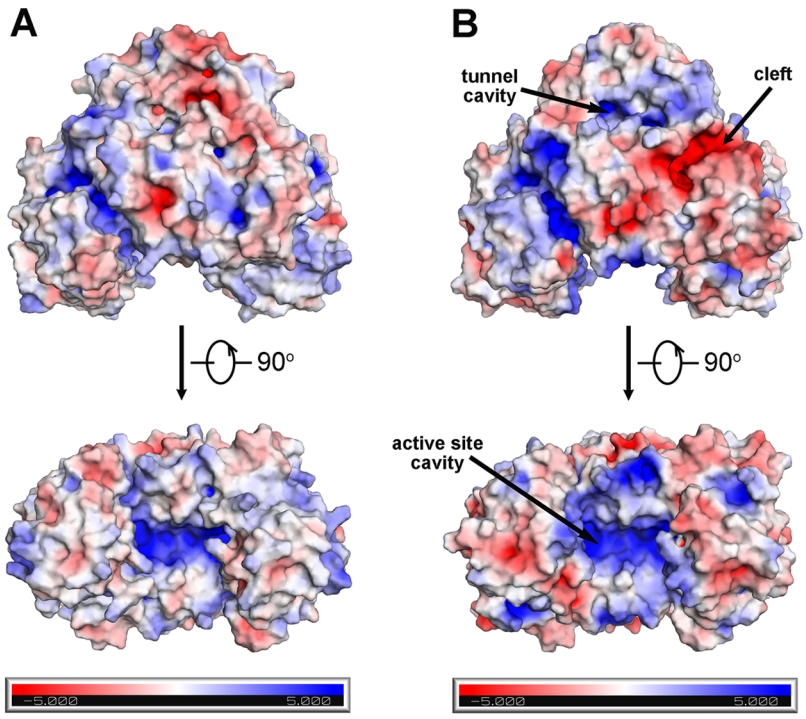

Figure 4. Electrostatic surface potential of LmFH isoforms. The upper and lower panels represent two orthogonal views of the electrostatic surface potential representation of LmFH-2 (A) and LmFH-1 (B).

similarity with an rmsd between 0.2 and 0.3 Å. The dimeric architecture of LmFH-1 (Figure 2B) is very similar to LmFH-2 (Figure 2A), with each monomer consisting of two domains arranged around the active site (Figure 2C).

The LmFH-1 monomer shows an α + β-fold with 23 β-strands and 20 α-helices organized in two domains, an N-terminal domain (Ala10 to Pro357) and a C-terminal domain (Thr367 to Leu549), connected by a linker (Asp358 to Lys366) that is found ordered in chains A and B and disordered in chains C and D (Figure 2C and Figure 3). The first residues (Met1 to Leu9 from chains A and B and Met1 to Glu11 from chains C and D) and the linker residues (Asp358 to Lys366 from chain C and Glu361 to Lys366 from chain D) were excluded from the structure due to the lack of interpretable electron density. The N-terminal domain is composed of two nonsequential subdomains 1 (Ala10 to Lys194 and Asp331 to Pro357) and 2 (Gly195 to Ala330) (Figure 2C). Subdomain 1 contains 11 β-strands and five α-helices folded in a β-sheet, two β-hairpins, and an α-helical region (Figure 2C and Figure 3). The subdomain 2 contains five β-strands and five α-helices folded in a β-sheet sandwiched by α-helices (Figure 2C and Figure 3). The C-terminal domain contains seven β-strands and nine α-helices and is folded into a β-barrel and an α-helical region (Figure 2C and Figure 3). The linker contains one α-helix (Figure 2B,C). The monomer has a [4Fe-4S] cluster bound to three cysteine residues (Cys114, Cys233, and Cys328) from the N-terminal domain with C-X_{118}-C-X_{94}-C motif.

The LmFH-1 dimer interface is stabilized by 48 hydrogen bonds, formed between 34 residues, the majority of which are from the N-terminal domain, with the exception of the residue Arg412 from the C-terminal domain (Table S2). The great majority of residues at the dimeric interface are conserved between LmFH-1 and LmFH-2 enzymes (Figure 3).

Additionally, *S*-2-thiomalate appears to be bound in all four LmFH-1 chains in the asymmetric unit. Interestingly, analyses of the difference electron density maps showed differential coordination of *S*-2-thiomalate to the catalytic [4Fe-4S] cluster in the different LmFH-1 chains. In chains A and B, the same double conformation of the *S*-enantiomer is observed as is found in the LmFH-2-thio structure (Figure 2D,E). However, in chains C and D, *S*-2-thiomalate appears to coordinate to the catalytic [4Fe-4S] in a single conformation (Figure 2E).

Structural Comparisons of LmFH-1 and LmFH-2. LmFH isoforms share 59% sequence identity (Figure 3) and show very similar overall structures with two domains arranged around the catalytic [4Fe-4S] cluster (Figure 2C). The superposition of Cα atoms between LmFHs monomers shows an rmsd of ∼0.7 Å for 514 Cα atoms, of the 540 and 532 residues comprising LmFH-1 and LmFH-2, respectively.

The electrostatic surface potential of the LmFHs dimers reveals that LmFH-1 has a negatively charged cleft located in the N-terminal domain, which is not observed in LmFH-2. On the other hand, the positively charged cavity that leads to the active site is a common feature of both LmFH isoforms (Figure 4).

The structural differences between LmFH-1 and LmFH-2 are found on the top of the protein comprised of residues from the N-terminus and in the C-terminal region. LmFH-1 has two α-helices (α19 and α20) inserted at the C-terminus in comparison with LmFH-2 (Figure 3). The first 25-plus residues of the N-terminus, which are not highly conserved and lack secondary structure (Figure 3), are of different lengths and of slightly different conformations in LmFH-1 and LmFH-2 (Figure 2C). Also, the first few elements of secondary structure are variable. LmFH-1 lacks an α-helix (α1 in LmFH-2) and has a β-hairpin comprised of β-strands (β2 and β3) that is connected by a longer loop than is found in LmFH-2 (Figures 2C and 3). Collectively these differences at the N-

DOI: 10.1021/acschembio.8b00972
ACS Chem. Biol. 2019, 14, 266−275

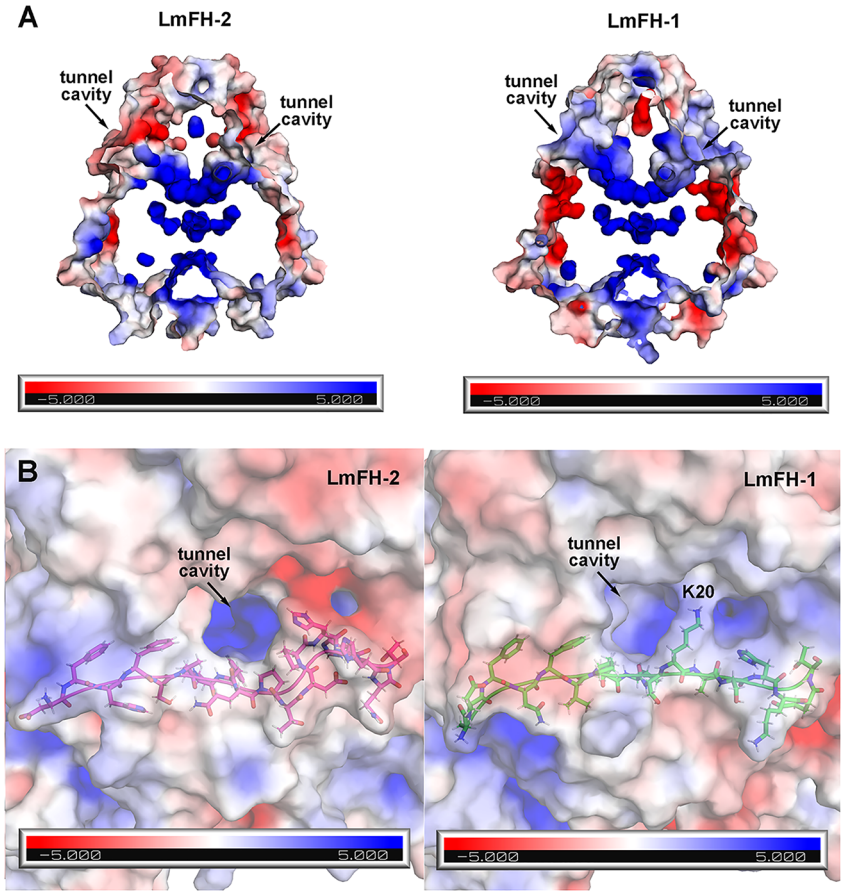

Figure 5. Positively charged cavity on the top of LmFHs. (A) This solvent exposed "top" cavity is the entrance of the positively charged tunnel that goes through the entire length of the proteins LmFH-2 (left panel) and LmFH-1 (right panel). (B) The left and right panels show the "top" cavities of LmFH-2 and LmFH-1, respectively. The N-terminal loop residues are shown in magenta (LmFH-2) and green (LmFH-1) sticks.

terminus lead to a more positively charged cavity at the top of LmFH-1 in comparison with LmFH-2 (Figures 4 and 5). This "top" cavity is the entrance to a tunnel that goes through the entire length of the LmFH-1 enzyme with an approximate diameter of 3−5 Å (Figure 5A). This tunnel is also found in the LmFH-2 structure and was described in detail previously.[7] In the LmFH-1 structure, the tunnel entrance is more solvent exposed. One residue, Lys20, which partially obscures the opening (Figure 5B), was modeled to calculate electrostatic surface potential but is disordered in the structure (Figure 5B). Possible functions of this tunnel have been considered[7] but are not established at this time.

The dimer interface of LmFHs is stabilized by hydrogen bonds between residues of the N-terminal domain from each monomer. However, the LmFH-1 dimer interface has one additional hydrogen bond between the N- and C-terminal domains (chain B residue Ser210 to chain A residue Arg412) (Table S2) that was not observed in LmFH-2.[7] This difference appears to be a conserved feature of mitochondrial FHs (Figure S3). The residues Ser210 and Arg412 of LmFH-1 are Ala and Lys, respectively, in LmFH-2 (Figure 3). In addition, LmFH isoforms have a [4Fe-4S] cluster bound to three cysteine residues with C^{114}-X_{118}-C^{233}-X_{94}-C^{328} (LmFH-1) and C^{133}-X_{118}-C^{252}-X_{93}-C^{346} (LmFH-2) motifs that are different by only one residue between the second and the third cysteine.

2-Thiomalate Binding Comparisons. As mentioned above, the *S*-enantiomer of 2-thiomalate was modeled in the electron density map of both LmFH structures (Figure 2D,E), where it occupies the substrate-binding site. Interestingly, *S*-2-thiomalate is bound to the unique Fe of the catalytic [4Fe-4S] cluster in two distinguishable conformations in LmFH-2 (Figure 6A) and in LmFH-1 chains A and B (Figure 6B). However, in LmFH-1 chains C and D, *S*-2-thiomalate is bound to the [4Fe-4S] cluster in a single conformation (Figure 6C). This single conformation is similar to *S*-malate binding mode observed in LmFH-2[7] and will be referred to as the canonical conformation (Figure 6C and Figure S4D). For *S*-malate, this "canonical conformation" involves coordination to the unique Fe of the [4Fe-4S] cluster *via* the C2-hydroxyl and C1-carboxyl oxygen atoms (Figure 6F and Figure S4D), and for *S*-2-thiomalate, this "canonical conformation" involves coordination to the unique Fe *via* the C2-thiol sulfur atom and C1-carboxyl oxygen atom (Figure 6C,D). Due to the difference in properties of sulfur versus oxygen, the Fe−S distance is longer (2.3 Å) than for Fe−O (1.95 Å). Also the C2-carboxylate to Fe distance is longer for *S*-2-thiomalate (2.66 Å) than for *S*-malate (2.47 Å) (Figure 6D,F). Importantly, the sulfur of *S*-2-thiomalate is very close (2.06 Å) to the proposed catalytic acid Asp135 (LmFH-2 numbering; Asp116 in LmFH-1) when Asp135 is in its canonical position, and we observe alternative conformations of both Asp135 and *S*-2-thiomalate that minimize this close interaction (Figure 6A,D). In the alternative conformation of *S*-2-thiomalate, the sulfur has moved away from Asp135/116 (LmFH-2/LmFH-1) into the position formerly occupied by the C2-carboxylate, and the carboxylate has swung down toward Arg454 in LmFH-1 and

DOI: 10.1021/acschembio.8b00972
ACS Chem. Biol. 2019, 14, 266−275

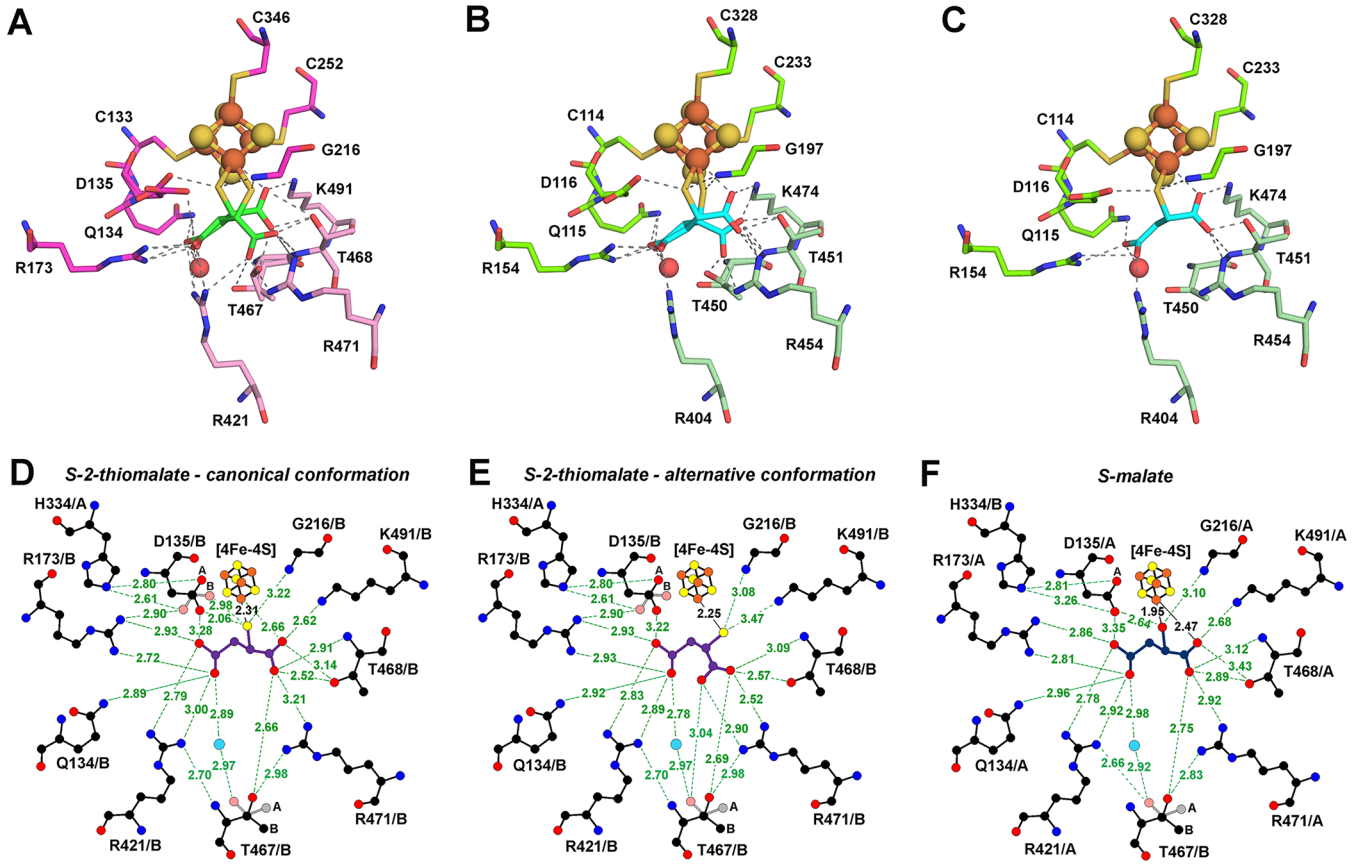

Figure 6. LmFHs active sites in a complex with *S*-2-thiomalate and *S*-malate. (A) Double conformation of *S*-2-thiomalate (green) in the active site of LmFH-2 from chain B. The residues of N- and C-terminal domains are shown in pink and light pink, respectively. (B) Double conformation of *S*-2-thiomalate (cyan) in the active site of LmFH-1 from chain B. The residues of N- and C-terminal domains are shown in green and light green, respectively. (C) Single conformation (canonical) of *S*-2-thiomalate (cyan) in the active site of LmFH-1 from chain C. The residues of N- and C-terminal domains are shown in green and light green, respectively. The [4Fe-4S] cluster is shown in orange (Fe) and yellow (S) spheres. The water molecule is shown in red sphere. (D) 2D representation of the interactions between *S*-2-thiomalate (purple; canonical conformation) and the active site residues in LmFH-2. (E) 2D representation of the interactions between *S*-2-thiomalate (purple; alternative conformation) and the active site residues in LmFH-2. (F) 2D representation of the interactions between *S*-malate (dark blue) and the active site residues in LmFH-2 (PDB code 5L2R). The double conformation of the residues Asp135 and Thr467 are labeled in parts A and B. The water molecule, C, N, O, Fe, and S atoms are shown in cyan, black, blue, red, orange, and yellow, respectively. The hydrogen bonds are shown as green dashed lines. Image created with LigPlot+.[17]

Arg471 in LmFH-2 (Figure 6A,B,E). In the chains of LmFH-1 that display two conformations of *S*-2-thiomalate (Figure 6B), the occupancies are ∼0.7 (canonical conformation) and ∼0.3 (alternative conformation). The LmFH-2 structure only displays the double conformation of *S*-2-thiomalate (Figure 6A) with occupancies of ∼0.5.

Despite the presence of multiple conformations of *S*-2-thiomalate, this inhibitor does contact the same residues that are involved in binding *S*-malate (Figure S4B–D and Figure 3). Additionally, the active site amino acids that interact with the inhibitor are fully conserved in class I FHs (Figure S3). Outside of the movement of Asp116/135 (LmFH-1/LmFH-2), other slight rearrangements, such as that of Arg404/421 and Thr450/467 (LmFH-1/LmFH-2), do not appear to be specific to *S*-2-thiomalate binding. The Thr467 double conformation was previously observed in the *S*-malate bound LmFH-2 structure,[7] and Arg404/421 (LmFH-1/LmFH-2) shows modest movement between LmFH-1 and LmFH-2 structures with *S*-2-thiomalate (Figure S4A). The canonical conformation of *S*-2-thiomalate is similar for both LmFHs, but the *S*-2-thiomalate alternative conformation is slightly different between LmFH-1 and LmFH-2 (Figure S4A).

Overall, our structures validate that *S*-2-thiomalate coordinates the unique Fe of the catalytic [4Fe-4S] cluster *via* its thiol moiety (∼ 2.3 Å), thus blocking the active site.

DISCUSSION

Class I parasitic FHs are important metabolic enzymes that contain an oxygen sensitive [4Fe-4S] cluster as a cofactor. Due to their involvement in core metabolic pathways such as the TCA cycle and succinate fermentation and given the profound structural differences with class II human FH, class I FHs hold potential as drug targets against leishmaniases, neglected tropical diseases that affect million of people worldwide. The ineffectiveness of leishmaniases drug therapies is the driving factor in the search for new drugs and new drug targets to fight these diseases.

This study identifies the small molecule 2-thiomalate, an analogue of the substrate *S*-malate, as a micromolar inhibitor of both LmFH isoforms. 2-Thiomalate has also been identified as a micromolar competitive inhibitor of class I FHs from *Trypanosoma cruzi* ($K_{i,malate}$ = 4.2 ± 0.5 μM for cytosolic isoform; $K_{i,malate}$ = 1.3 ± 0.1 μM for mitochondrial isoform) and *Plasmodium falciparum* (K_i = 0.32 ± 0.03 μM for *S*-malate;

DOI: 10.1021/acschembio.8b00972
ACS Chem. Biol. 2019, 14, 266–275

K_i = 0.55 ± 0.05 μM for fumarate) but does not inhibit class II human FH.[10,11] To our knowledge, 2-thiomalate is the first selective inhibitor of class I FHs.

In order to investigate the mechanism of inhibition, we solved the crystal structures of both LmFH isoforms in a complex with 2-thiomalate. Our structures show a high level of structural similarity between mitochondrial LmFH-1 and cytosolic LmFH-2 isoforms and reveal the mode of inhibitor-binding. Notably, inhibition and crystallization assays were performed using the racemic mixture of *RS*-2-thiomalate, but our structural data provide no evidence that the *R*-enantiomer of 2-thiomalate binds to either LmFH enzyme. Thus, the IC_{50} values measured here using a ∼50:50 racemic mixture of *RS*-2-thiomalate are likely to be an underestimate of 2-thiomalate's potency. Importantly, 2-thiomalate is already Food and Drug Administration (FDA)-approved for delivery of gold (as sodium auro-2-thiomalate) for the treatment of arthritis. Auro-2-thiomalate is thought to dissociate in the plasma to protein-bound gold and free 2-thiomalate. The therapeutic target of the gold is unknown. Treatment with auro-2-thiomalate can involve weekly injections of 10 mg up to a cumulative dose of 1 g. Toxicity associated with auro-2-thiomalate appears to be very low.[18,19] Given the low toxicity, low micromolar/high nanomolar inhibition by the commercially available, FDA-approved 2-thiomalate warrants further investigation.

Our crystal structures confirmed our expectation that *S*-2-thiomalate binds to class I LmFH-1 and LmFH-2 through the coordination of its thiol group to the unique Fe of the catalytic [4Fe-4S] cluster. This binding mode is in agreement with hard−soft acid base theory,[20] wherein the [4Fe-4S] cluster, a Lewis acid, binds strongly to soft base such as thiol group. We were not expecting to find two conformations of *S*-2-thiomalate bound to the cluster, but in retrospect, the double conformation of *S*-2-thiomalate does make sense. Although *S*-2-thiomalate is a very close mimic of substrate *S*-malate, the active site is so tightly packed that even a small difference, such as bigger atomic radius of sulfur compared to oxygen, has an impact. We find that the second, "noncanonical" conformation of *S*-2-thiomalate relieves the close distance between the sulfur of *S*-2-thiomalate and the carboxylate of catalytic residue Asp135/116 (LmFH-2/LmFH-1). Both conformations of *S*-2-thiomalate are expected to be inhibitory and block substrate binding, as both coordinate the cluster and both interact with substrate-binding residues. The observation that *S*-2-thiomalate does not inhibit class II FHs is likely due to the lack of a [4Fe-4S] cluster in that class of enzymes. Our data support the importance of a thiolate-cluster coordination to *S*-2-thiomalate's inhibitory properties. In addition, due to active site conservation in class I FHs (Figure S3), inhibitors of LmFHs may also be selective inhibitors that target tropical diseases caused by other trypanosomatids, such as *Trypanosoma cruzi* and *Trypansoma brucei*. Of course, each case should be evaluated separately as there are complications associated with treating different tropical diseases. For example, treatment of stage II human African trypanosomiasis (sleeping sickness) requires drugs to cross the blood-brain barrier. Although one drug may not fit all, the findings that we present here will hopefully lead to additional studies aimed at evaluating the promise of 2-thiomalate for treatment of one or more tropical diseases.

In summary, this work reveals the mechanism of action of *S*-2-thiomalate in class I FHs; this inhibitor coordinates the unique Fe of the [4Fe-4S] cluster and blocks the active site. This inhibitor provides selectivity by targeting the [4Fe-4S] cluster found in parasitic class I FHs but absent in human class II FH. In addition, our data specify LmFH isoforms as attractive drug targets for development of new therapies against leishmaniasis. These findings, together with the low toxicity of 2-thiomalate to humans,[18] suggest the inhibitor *S*-2-thiomalate as a promising hit compound for the development of therapeutics to fight tropical diseases, such as leishmaniases, Chagas diseases, sleeping sickness, and malaria.

METHODS

Expression and Purification of LmFH Isoforms. Recombinant LmFH-1 (mitochondrial isoform) and LmFH-2 (cytosolic isoform) were expressed in *E. coli* T7 express and purified by nickel affinity chromatography as described previously[9] at 4 °C in an MBraun anaerobic glovebox. For crystallization assays, the purification of LmFH isoforms was performed with 1 mM dithiothreitol (DTT) in all buffers.

Inhibition Assays with 2-Thiomalate. Inhibition analyses of LmFH-1 and LmFH-2 by *RS*-2-thiomalate (Alfa Aesar) were carried out in an MBraun anaerobic glovebox. The fumarate production and consumption were measured at 250 nm ($\varepsilon_{250nm}^{fumarate}$ = 1 450 M^{-1} cm^{-1}) and 300 nm ($\varepsilon_{300nm}^{fumarate}$ = 36.6 M^{-1} cm^{-1}), respectively, at RT in a USB 4000 fiber optic spectrometer (Ocean Optics). Inhibition assays were performed in a reaction mixture containing 50 mM Tris, pH 9, 150 mM NaCl with substrate (3 mM *S*-malate, 3 or 6 mM fumarate) and inhibitor (0 to 1 mM *RS*-2-thiomalate) in a total volume of 1 mL. The reaction was started by adding 2.5 μL of enzyme (∼6 mg mL^{-1} of LmFH-1 or ∼4 mg mL^{-1} of LmFH-2, both in 50 mM Tris, pH 8.5, 150 mM NaCl). The IC_{50} was determined from the dose−response equation (eq 1) fitted to the experimental data obtained by varying the concentration of *RS*-2-thiomalate.

$$\text{Inhibition}\ (\%) = I_{min}(\%) + \frac{I_{max}(\%) - I_{min}(\%)}{1 + 10^{(\log IC_{50} - \log[I])h}} \quad (1)$$

where the inhibition (%) is written as a function of log [I], the log of inhibitor concentration, I_{min} (%) is the minimum inhibition, I_{max} (%) is the maximum inhibition, IC_{50} is the half maximal inhibitory concentration, and *h* is the Hill coefficient. Data were fitted using Origin software (http://www.originlab.com).

Crystallization of LmFH-2 with 2-Thiomalate. LmFH-2 crystals were obtained by the hanging drop vapor diffusion method at RT in a Coy anaerobic chamber as described previously.[7] LmFH-2 crystallizes using precipitate tacsimate, which is composed of a mixture of titrated organic acid salts[21] that contains the substrate malate and inhibitors malonate and succinate. To obtain LmFH-2 crystals only in the presence of 2-thiomalate, the ligands malate, malonate, and succinate were removed from the original tacsimate composition, and *RS*-2-thiomalate was added (Table S3). Drops were prepared by mixing 1 μL of protein solution (5−10 mg mL^{-1} in 50 mM Tris, pH 8.5, 150 mM NaCl, 1 mM DTT, 10 mM *RS*-2-thiomalate), 1 μL of reservoir solution (8−12% (v/v) polyethylene glycol (PEG) 3 350, 5−10 mM ammonium citrate tribasic, 8−16 mM sodium acetate trihydrate, 10−20 mM sodium formate, 3.2−6.4 mM ammonium tartrate dibasic, 6−12 mM *RS*-2-thiomalate, pH 5) and equilibrating against 400 μL of reservoir solution. The crystals were transferred to a cryoprotectant solution (25% (v/v) glycerol, 18% (v/v) PEG 3 350, 20 mM ammonium citrate tribasic, 32 mM sodium acetate trihydrate, 40 mM sodium formate, 12.8 mM ammonium tartrate dibasic, 24 mM *RS*-2-thiomalate, pH 5) and flash-cooled in liquid nitrogen in the Coy chamber.

Crystallization of LmFH-1 with 2-Thiomalate. LmFH-1 crystals were obtained by hanging drop vapor diffusion method at RT in a Coy anaerobic chamber. Drops were prepared by mixing 1 μL of protein solution (5−10 mg mL^{-1} in 50 mM Tris pH 8.5, 150 mM NaCl, 1 mM DTT, 10 mM *RS*-2-thiomalate) and 1 μL of reservoir solution (0.1 M HEPES pH 7.5, 1.9−2.2 M ammonium sulfate, 3−4%

DOI: 10.1021/acschembio.8b00972
ACS Chem. Biol. 2019, 14, 266−275

(v/v) polyethylene glycol (PEG) 400, 10 mM *RS*-2-thiomalate), and equilibrated against 400 μL of reservoir solution. After 1 day, brownish square crystals were obtained. The crystals were transferred to a cryoprotectant solution (98 mM HEPES pH 7.5, 2.4 M ammonium sulfate, 9.8 mM *RS*-2-thiomalate, 19.6% (v/v) glycerol) and flash-cooled in liquid nitrogen in the Coy chamber.

Data Collection and Structure Determination of LmFH Isoforms. Data collection was performed at 24-ID-C beamline of the Advanced Photon Source. Diffraction data were processed and scaled using HKL2000[22] with the CC1/2 value used to determine the resolution cutoff. The LmFH-1 data were initially processed in the space group $P42_12$, but phenix.xtriage[23] analyses indicated that the intensity statistics looked unusual, suggesting crystal twinning. The inability to find a molecular replacement solution in the space group $P42_12$ also suggested the possibility of twinned crystal and/or incorrect space group assignment. Consequently, the diffraction data were reprocessed in the space groups *P*4, *P*222, *P*2, and *C*2. A molecular replacement solution was only possible in the space group $P2_1$. Analyses of the intensity statistics in $P2_1$ by phenix.xtriage[23] indicated that LmFH-1 crystals were pseudomerohedrally twinned with the twin fraction of 0.457 (Britton analyses[24]), and twin law h, -k, -l. The crystal structures of LmFH-1 and LmFH-2 in a complex with 2-thiomalate were solved by molecular replacement techniques implemented in Phaser.[25] The coordinates of the LmFH-2 structure (PDB ID code 5L2R[7]) was used to obtain the initial phases. Following molecular replacement, simulated annealing was performed in phenix.refine[23] to remove model bias. Model building and addition of water molecules using Coot[26] was iterated with refinement in phenix.refine,[23] using torsion NCS (noncrystallographic symmetry) restraints, TLS (translation, libration, and screw), and positional and individual B-factor refinement, with 2-thiomalate geometry restraints generated by phenix.elbow.[23] The LmFH-1 structure was refined with twin law h, -k, -l. The LmFH-2 final model contains two polypeptide chains, two [4Fe-4S] clusters, two *S*-2-thiomalate molecules, and 821 water molecules. The polypeptide chains A and B include, of 568 residues, residues from Asp28 to Pro375 and Thr385 (chain A)/Ser386 (chain B) to Ala568. The LmFH-1 final model contains four polypeptide chains, four [4Fe-4S] clusters, four *S*-2-thiomalate molecules, eight glycerol molecules, two di(hydroxyethyl)ether (PEG) molecules, five triethylene glycol (PGE) molecules, two tetraethylene glycol (PG4) molecules, one pentaethylene glycol (1PE) molecule, and 870 water molecules. The polypeptide chains (chains A, B, C and D) include, of 549 residues, residues from Ala10 to Leu549, Ala10 to Leu549, Phe12 to Pro357 and Thr367 to Gln548, and Phe12 to Lys360 and Thr367 to Gln548, respectively. The data collection and refinement statistics are summarized in Table S1. Figures were created with PyMol software.[27] The electrostatic surface potentials were calculated using the Adaptive Poisson−Boltzmann Solver (APBS)[28] plugin implemented in PyMol, using default parameters. Crystallographic software packages were compiled by SBGrid.[29]

■ ASSOCIATED CONTENT

Supporting Information

. The Supporting Information is available free of charge on the ACS Publications website at DOI: 10.1021/acschembio.8b00972.

Data collection and refinement statistics of LmFH isoforms, hydrogen bonds formed between residues of chains A and B from LmFH-1, tacsimate composition and its variation in the presence of 2-thiomalate, *RS*-thiomalate characterization and use, stereoview of *R*-2-thiomalate modeled in the active site of LmFH-2, sequence alignment of mitochondrial class I FH isoforms, and stereoview of LmFHs active sites in a complex with *S*-2-thiomalate an *S*-malate (PDF)

Accession Codes

The structures of LmFH-1 and LmFH-2 bound to inhibitor *S*-2-thiomalate have been deposited in the Protein Data Bank with accession codes 6MSO and 6MSN, respectively.

■ AUTHOR INFORMATION

Corresponding Authors

*E-mail: cdrennan@mit.edu.
*E-mail: cristy@fcfrp.usp.br.

ORCID

Patricia R. Feliciano: 0000-0003-3853-115X
Catherine L. Drennan: 0000-0001-5486-2755

Author Contributions

P.R.F. designed and performed experiments, analyzed the data, and wrote the manuscript. M.C.N. and C.L.D. supervised the research, contributed to data analysis, and wrote the manuscript.

Notes

The authors declare no competing financial interest.

■ ACKNOWLEDGMENTS

We thank Mary C. Andorfer for assistance with the collection of the circular dichroism spectra of *RS*-2-thiomalate. We acknowledge financial support from Fundação de Amparo a Pesquisa do Estado de São Paulo (FAPESP), Grants 2013/14988-8 and 2014/22246-4 (P.R.F.) and Grant 2008/08262-6 (M.C.N.), and from the National Institute of General Medical Sciences of the National Institutes of Health Grant R35 GM126982 (C.L.D.). C.L.D. is a Howard Hughes Medical Institute Investigator. This work is based upon research conducted at the Northeastern Collaborative Access Team beamlines, which are funded by the National Institute of General Medical Sciences of the National Institutes of Health (Grant P41 GM103403). The Pilatus 6M detector on 24-ID-C beamline is funded by a National Institutes of Health-ORIP HEI grant (Grant S10 RR029205). This research used resources of the Advanced Photon Source, a U.S. Department of Energy (DOE) Office of Science User Facility operated for the DOE Office of Science by Argonne National Laboratory under Contract No. DE-AC02-06CH11357.

■ REFERENCES

(1) Aagaard-Hansen, J., Nombela, N., and Alvar, J. (2010) Population movement: a key factor in the epidemiology of neglected tropical diseases. *Trop. Med. Int. Health 15*, 1281−1288.

(2) Argaw, D., Mulugeta, A., Herrero, M., Nombela, N., Teklu, T., Tefera, T., Belew, Z., Alvar, J., and Bern, C. (2013) Risk Factors for Visceral Leishmaniasis among Residents and Migrants in Kafta-Humera, Ethiopia. *PLoS Neglected Trop. Dis. 7*, e2543.

(3) Field, M. C., Horn, D., Fairlamb, A. H., Ferguson, M. A. J., Gray, D. W., Read, K. D., De Rycker, M., Torrie, L. S., Wyatt, P. G., Wyllie, S., and Gilbert, I. H. (2017) Anti-trypanosomatid drug discovery: an ongoing challenge and a continuing need. *Nat. Rev. Microbiol. 15*, 217.

(4) Coustou, V., Besteiro, S., Riviere, L., Biran, M., Biteau, N., Franconi, J. M., Boshart, M., Baltz, T., and Bringaud, F. (2005) A mitochondrial NADH-dependent fumarate reductase involved in the production of succinate excreted by procyclic *Trypanosoma brucei*. *J. Biol. Chem. 280*, 16559−16570.

(5) Yogev, O., Yogev, O., Singer, E., Shaulian, E., Goldberg, M., Fox, T. D., and Pines, O. (2010) Fumarase: A Mitochondrial Metabolic Enzyme and a Cytosolic/Nuclear Component of the DNA Damage Response. *PLoS Biol. 8*, e1000328.

(6) Coustou, V., Biran, M., Besteiro, S., Riviere, L., Baltz, T., Franconi, J. M., and Bringaud, F. (2006) Fumarate is an essential

DOI: 10.1021/acschembio.8b00972
ACS Chem. Biol. 2019, 14, 266−275

intermediary metabolite produced by the procyclic *Trypanosoma brucei*. *J. Biol. Chem. 281*, 26832−26846.
(7) Feliciano, P. R., Drennan, C. L., and Nonato, M. C. (2016) Crystal structure of an Fe-S cluster-containing fumarate hydratase enzyme from *Leishmania major* reveals a unique protein fold. *Proc. Natl. Acad. Sci. U. S. A. 113*, 9804−9809.
(8) Pereira de Padua, R. A., and Nonato, M. C. (2014) Cloning, expression, purification, crystallization and preliminary X-ray diffraction analysis of recombinant human fumarase. *Acta Crystallogr., Sect. F: Struct. Biol. Commun. 70*, 120−122.
(9) Feliciano, P. R., Gupta, S., Dyszy, F., Dias-Baruffi, M., Costa-Filho, A. J., Michels, P. A. M., and Nonato, M. C. (2012) Fumarate hydratase isoforms of *Leishmania major*: Subcellular localization, structural and kinetic properties. *Int. J. Biol. Macromol. 51*, 25−31.
(10) de Padua, R. A. P., Kia, A. M., Costa-Filho, A. J., Wilkinson, S. R., and Nonato, M. C. (2017) Characterisation of the fumarate hydratase repertoire in *Trypanosoma cruzi*. *Int. J. Biol. Macromol. 102*, 42−51.
(11) Jayaraman, V., Suryavanshi, A., Kalale, P., Kunala, J., and Balaram, H. (2018) Biochemical characterization and essentiality of *Plasmodium* fumarate hydratase. *J. Biol. Chem. 293*, 5878−5894.
(12) Kinsella, B. T., and Doonan, S. (1986) Nucleotide sequence of a cDNA coding for mitochondrial fumarase from human liver. *Biosci. Rep. 6*, 921−929.
(13) Saunders, E. C., Ng, W. W., Chambers, J. M., Ng, M., Naderer, T., Kromer, J. O., Likic, V. A., and McConville, M. J. (2011) Isotopomer Profiling of *Leishmania mexicana* Promastigotes Reveals Important Roles for Succinate Fermentation and Aspartate Uptake in Tricarboxylic Acid Cycle (TCA) Anaplerosis, Glutamate Synthesis, and Growth. *J. Biol. Chem. 286*, 27706−27717.
(14) Cer, R. Z., Mudunuri, U., Stephens, R., and Lebeda, F. J. (2009) IC50-to-K-i: a web-based tool for converting IC50 to K-i values for inhibitors of enzyme activity and ligand binding. *Nucleic Acids Res. 37*, W441−W445.
(15) Corpet, F. (1988) Multiple sequence alignment with hierarchical-clustering. *Nucleic Acids Res. 16*, 10881−10890.
(16) Gouet, P., Courcelle, E., Stuart, D. I., and Metoz, F. (1999) ESPript: analysis of multiple sequence alignments in PostScript. *Bioinformatics 15*, 305−308.
(17) Laskowski, R. A., and Swindells, M. B. (2011) LigPlot+: Multiple Ligand-Protein Interaction Diagrams for Drug Discovery. *J. Chem. Inf. Model. 51*, 2778−2786.
(18) Rudge, S. R., Perrett, D., and Swannell, A. J. (1984) Free thiomalate in plasma and urine of patients receiving sodium aurothiomalate. *Ann. Rheum. Dis. 43*, 66−69.
(19) Jellum, E., Aaseth, J., and Munthe, E. (1977) Is mechanism of action during treatment of rheumatoid-arthritis with penicillamine and gold thiomalate same. *Proc. R. Soc. Med. 70*, 136−139.
(20) Pearson, R. G. (1963) Hard and soft acids and bases. *J. Am. Chem. Soc. 85*, 3533−3539.
(21) McPherson, A., and Cudney, B. (2006) Searching for silver bullets: An alternative strategy for crystallizing macromolecules. *J. Struct. Biol. 156*, 387−406.
(22) Otwinowski, Z., and Minor, W. (1997) Processing of X-ray diffraction data collected in oscillation mode. *Methods Enzymol. 276*, 307−326.
(23) Adams, P. D., Afonine, P. V., Bunkoczi, G., Chen, V. B., Davis, I. W., Echols, N., Headd, J. J., Hung, L. W., Kapral, G. J., Grosse-Kunstleve, R. W., McCoy, A. J., Moriarty, N. W., Oeffner, R., Read, R. J., Richardson, D. C., Richardson, J. S., Terwilliger, T. C., and Zwart, P. H. (2010) PHENIX: a comprehensive Python-based system for macromolecular structure solution. *Acta Crystallogr., Sect. D: Biol. Crystallogr. 66*, 213−221.
(24) Lebedev, A. A., Vagin, A. A., and Murshudov, G. N. (2006) Intensity statistics in twinned crystals with examples from the PDB. *Acta Crystallogr., Sect. D: Biol. Crystallogr. 62*, 83−95.
(25) McCoy, A. J., Grosse-Kunstleve, R. W., Adams, P. D., Winn, M. D., Storoni, L. C., and Read, R. J. (2007) Phaser crystallographic software. *J. Appl. Crystallogr. 40*, 658−674.
(26) Emsley, P., Lohkamp, B., Scott, W. G., and Cowtan, K. (2010) Features and development of Coot. *Acta Crystallogr., Sect. D: Biol. Crystallogr. 66*, 486−501.
(27) Delano, W. L. *The PyMOL Molecular Graphics System*, DeLano Scientific LLC, San Carlos, CA.
(28) Baker, N. A., Sept, D., Joseph, S., Holst, M. J., and McCammon, J. A. (2001) Electrostatics of nanosystems: Application to microtubules and the ribosome. *Proc. Natl. Acad. Sci. U. S. A. 98*, 10037−10041.
(29) Morin, A., Eisenbraun, B., Key, J., Sanschagrin, P. C., Timony, M. A., Ottaviano, M., and Sliz, P. (2013) Collaboration gets the most out of software. *eLife 2*, 6.

DOI: 10.1021/acschembio.8b00972
ACS Chem. Biol. 2019, 14, 266−275